Homogenization of ultrathin metallo-dielectric structures leading to transmission conditions at an equivalent interface

Agnes Maurel, Jean-Jacques Marigo, Abdelwaheb Ourir

HAL Id: hal-01657078

https://polytechnique.hal.science/hal-01657078

Submitted on 6 Dec 2017

Homogenization of ultra thin metallo-dielectric structures leading to transmission conditions at an equivalent interface

AGNÈS MAUREL [1], **JEAN -JACQUES MARIGO**[2], **AND ABDELWAHEB OURIR**[1]

[1] *Institut Langevin, 1 rue Jussieu, 75005 Paris, France*
[2] *LMS, Ecole Polytechnique, Route de Saclay, 91128 Palaiseau, France*
[*] *Corresponding author: agnes.maurel@espci.fr*

Compiled March 19, 2016

We present a method of homogenization of thin metallo-dielectric structures as used in the design of artificial surfaces, or metasurfaces. The approach is based on a so-called matched asymptotic expansion technique, leading to parameters being characteristic of an equivalent interface associated to jump conditions. It is applied to an array of metal strips on top of a metal-backed dielectric slab, with the strips having a small but possibly finite thickness. Solving the equivalent problem provides explicit expressions (i) of the reflection coefficient for a wave at oblique incidence and (ii) of the dispersion relation of the surface waves. The results are shown to be in agreement with results coming from the transmission line theory in the limit of vanishing thickness of the metallization and for normal incidence of the wave. The influence of the finite thickness of the metallization is exemplified and validated by comparison with full wave simulations.

1. INTRODUCTION

It is nowadays admitted that the properties of bulk structures involving a periodic arrangement of scatterers at the subwavelength scale are correctly captured by classical homogenization techniques, *e.g.* [1, 2]. In general, the problem ends with effective permittivity and effective permeability able to describe the material at the macroscale, even in complex cases including non local effects [3], bianisotropy at small scale [4] or resonances within the unit cell [5]. However, these homogenization techniques fail when the thickness of the structures becomes of the order of (or smaller than) the wavelength and there is a lack in approaches able to give an effective behavior of ultrathin devices within a rigorous mathematical framework (an enlightening review can be found in Ref. [6]).

Starting in the 1970s, homogenization techniques based on matched asymptotic expansions have been developed, mainly for static problems, and adapted more recently to wave problems in few contexts, as in the context of seismic waves [7, 8]. These approaches have the same ingredients as the classical homogenization, the two scale method and the asymptotic expansion, but they explicitly account for the subwavelength thickness of the device. This is because two different expansions are used in the near and far fields of the scatterers, which are connected using so-called matching conditions.

In this paper, we present an interface homogenization based on such matched asymptotic expansion technique as developed in the static case in [9, 10]. We focus on the case of artificial metal-dielectric structures, formed by a periodic arrangement of metallic components separated from a metallic ground plate by a dielectric substrate. Such surfaces are known as frequency selective surfaces (FSS), artificial magnetic conductors (AMC) or high impedance surfaces (HIS), and they have found numerous applications in telecommunication, for instance in the design of antennas. There is currently renewed interest in the context of the metamaterials for these so-called metasurfaces, because of their unconventional properties to interact with light, see the recent review [11]. Among the various functionalities of these artificial surfaces, their abilities to modify the reflection phase and the band gap structure (see *e.g.*[12]) have been revisited to realize metasurfaces controlling the reflected wave within generalized Snell's Descartes laws [13, 14] and realizing perfect absorbers [15].

To describe such devices, the main step in our approach is to replace the metallic array by an equivalent interface associated to jump conditions involving interface parameters, afterwards the propagation in the grounded dielectric substrate is explicitly accounted for. These interface parameters are determined by solving elementary problems (or unit cell problems) which allows to deal with complex geometries of the array and of the interface with the dielectric. The transmission line theory has been shown to accurately describe the propagation in such devices but the approach is limited to simple geometries of the metallization for which a capacitive or an inductive structure is recognized [16]. Also, it neglects the thin but possibly non zero thickness of the metallization, and the influence of this thickness will be regarded in the present study. In fact, although the metallization, realized by means of mechanical or chemical etching, may lead to very thin metallic parts, accounting for a non vanishing thickness adds an extra flexibility to the design of the metasurface. Besides, in practical realizations, the relative metal thickness ke (with e the metal thickness and k the wavenumber of the incident wave) may be not negligible, for instance $ke \sim 0.2 - 0.5$ are used in Refs. [14, 17].
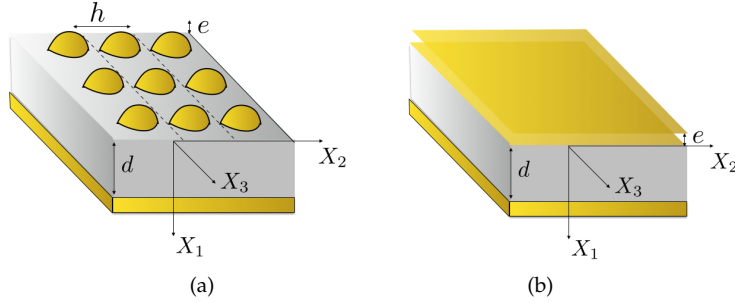

Fig. 1. (a) Typical geometry of the artificial surface composed of a metallic array supported by a metal backed dielectric substrate, (b) equivalent thin interface on the metal backed dielectric substrate.

The paper is organized as follow. In Section 2, the matched asymptotic expansion is presented for transverse magnetic polarization (TM). Particularities due to the presence of the air/dielectric interface in addition to the presence of the metallic array are stressed. The problem ends with transmission, or jump conditions being expressed in terms of interface parameters, among which the volume fraction of metal in the array, Eqs. (24). The interface parameters are given unambiguously by means of the resolution of static unit cell problems being expressed in the near field of the array, Eqs. (15)-(16), and unambiguously is meant without any retrieval procedure. The section 3 presents results from full wave simulations validating our homogenized model in the simplest geometry of metallic strips, for which explicit expressions of the effective parameters are given, Eqs. (23). This is done by inspecting the variations of the reflection phase with the frequency. For a metallic array with zero thickness, the agreement with the transmission line theory is demonstrated at normal incidence, where the two approaches can be compared. Next, the sensitivity of the reflection phase on the array thickness is illustrated, leading to an additional flexibility in the central frequency of the in-phase reflection without affecting much the useful bandwidth. We end the validation by inspecting the dispersion relation of the guided waves, Eq. (27), and we show that increasing the array thickness allows for a control in the band gap structure of the guided waves. Finally, two appendices collect minor results, (i) results and comments on the interface parameters in TM polarization and (ii) the derivation of the interface parameters and the reflection coefficient in the case of transverse electric polarization (TE). This polarization is of less interest in the present case since it does not allow for much flexibility in the reflection phase and in the band gap structure.

Throughout the paper, the time dependence is $e^{i\omega t}$, with ω the frequency and t the time.

2. HOMOGENIZATION OF THE STRUCTURED METALLIC ARRAY

The idea is to replace the metallic array of thickness e by an interface, and it is the main problem to determine the effective conditions to be applied at this equivalent interface. To that aim, we first consider the problem of the metallic array sandwiched between the air and the dielectric with relative permittivity ϵ_r (the ground plane is disregarded at this stage).

We start with the wave equation written for the magnetic field $H(\mathbf{X})$ ($\mathbf{X} = (X_1, X_2)$) being polarized along $\mathbf{e}_3$

$$\text{div}\left[\frac{1}{\epsilon}\boldsymbol{\nabla} H\right] + k^2 H = 0, \tag{1}$$

with $k = \sqrt{\epsilon_0\mu_0}\omega$ the wavenumber in the air, ϵ the relative permittivity being dependent on space (the relative permeability for the dielectric is 1). The boundary conditions at the air/dielectric interface are the continuities of H and of $1/\epsilon\boldsymbol{\nabla}H.\mathbf{n}$, and the boundary condition on the metal is $\boldsymbol{\nabla}H.\mathbf{n} = 0$; note that this latter condition for a perfectly conducting metal has been regarded in detail when a thin structure is considered [18, 19]. Next, we define the field $\boldsymbol{C}$, with $\boldsymbol{\nabla}H = k\epsilon\boldsymbol{C}$, so that the Eq. (1) is written

$$\text{div}\boldsymbol{C} + kH = 0, \quad \boldsymbol{C} \equiv \frac{1}{k\epsilon}\boldsymbol{\nabla}H, \tag{2}$$

with boundary conditions being now the continuities of H and of $\boldsymbol{C}.\mathbf{n}$ at the air/dielectric interface, and $\boldsymbol{C}.\mathbf{n} = 0$ on the metal. Incidentally, it is easy to see that the electric field $\mathbf{E} = (E_1, E_2, 0)$ can be deduced from $\boldsymbol{C}$, using

$$C_1 = -i\sqrt{\epsilon_0\mu_0}\,E_2, \quad C_2 = i\sqrt{\epsilon_0\mu_0}\,E_1. \tag{3}$$

As in classical homogenization, we work using two dimensionless systems of coordinates, $\mathbf{x} = (x_1, x_2)$ and $\mathbf{y} = (y_1, y_2)$, being deduced from $\mathbf{X}$ by the relations $\mathbf{x} = k\mathbf{X}$ and $\mathbf{y} = \mathbf{X}/h$, and we define the small parameter

$$\eta = kh \ll 1.$$

Figs. 2 show the resulting rescaling of the unit cell in $\mathbf{x}$ and $\mathbf{y}$ coordinates. In the (y_1, y_2) plane, we define $\mathsf{Y}^+ = [0, y_1^m] \times [0, 1]$ and $\mathsf{Y}^- = [-y_1^m, 0] \times [0, 1] \backslash \mathsf{S}$, where S corresponds to the metallic part (and we denote $\mathcal{S}$ its volume); then $\mathsf{Y} = \mathsf{Y}^- \cup \mathsf{Y}^+$. The value of y_1^m is incidental, since only the limit $y_1^m \to \infty$ will be considered. Finally, for a function being discontinuous at $x_1 = 0$, we use the notations

$$\begin{cases} \overline{f}(0) \equiv \frac{1}{2} \left[f(0^+) + f(0^-) \right], \\[2mm] [\![f]\!] \equiv f(0^+) - f(0^-). \end{cases}$$
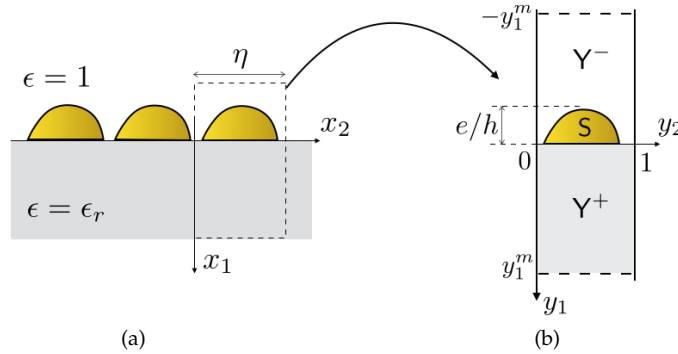

Fig. 2. Geometry and dimension of the metallic array between the air and the dielectric (a) in the (x_1, x_2) space and (b) in the (y_1, y_2) space.

A. Expansions of the solution in the near and far fields

The dependance of the field H on the systems of coordinates $\mathbf{x}$ and $\mathbf{y}$ is pertinent or not depending on how close we are from the array. Sufficiently far away, say in the far field, only the propagating field exists and it is associated to variations $|\nabla H(\mathbf{X})| \sim kH(\mathbf{X})$. With $H(\mathbf{x}) = H(\mathbf{X})$, the coordinates $\mathbf{x}$ naturally account for these variations, with $|\nabla_{\mathbf{x}} H(\mathbf{x})| \sim H(\mathbf{x})$ by construction. To the contrary, in the near field, we have to account for (i) the rapid variations of the evanescent field, typically associated to the scale h and (ii) the slow variations associated to the propagating field along X_2, say the condition of the pseudo-periodicity. The rapid variations are naturally accounted for with the coordinates $\mathbf{y}$ and to account for the slow variations, we keep x_2 as an additional coordinate, leading to $H(X) = H(\mathbf{y}, x_2)$ in the near field.

We now define the expansions in the far field

$$H = H^0(\mathbf{x}) + \eta H^1(\mathbf{x}) + \dots,$$

$$C = C^0(\mathbf{x}) + \eta C^1(\mathbf{x}) + \dots, \tag{4}$$

and the expansions in the near field

$$H = h^0(\mathbf{y}, x_2) + \eta h^1(\mathbf{y}, x_2) + \dots,$$

$$C = \mathbf{c}^0(\mathbf{y}, x_2) + \eta \mathbf{c}^1(\mathbf{y}, x_2) \dots. \tag{5}$$

As in the classical homogenization, the fields h^n and c^n, $n = 0, \dots$, are assumed to be periodic with respect y_2 and this is not meaningless in the present context since the condition of pseudo-periodicity is handled by the variable x_2. Thus, we recognize Floquet type solutions for (h^n, c^n). The Eqs. (2) will be written at the orders η^{-1} and η^0 in the near field and at the order η^0 and η^1 in the far field, using the differential operators

$$\begin{cases} \nabla \to k\nabla_{\mathbf{x}}, & \text{in the far field,} \\[2mm] \nabla \to k \left[\dfrac{1}{\eta} \nabla_{\mathbf{y}} + \dfrac{\partial}{\partial x_2} \mathbf{e}_2 \right], & \text{in the near field,} \end{cases} \tag{6}$$

afterwards matching conditions will be applied to connect the fields in the two regions. The leading order solution refers to the solution found at dominant order and the first order solution to the solution obtained at the next order.

Finally, something has to be said on the variation of ϵ. In the far field, it is equal to $\epsilon^- = 1$ for $x_1 < 0$ and equal to $\epsilon^+ = \epsilon_r$ for $x_1 > 0$; in the near field, it varies in a more complex way depending on the geometry of the array and on the shape of the air/dielectric interface. It is denoted $\epsilon(\mathbf{y})$ in the following, with

$$\epsilon(\pm\infty, y_2) = \epsilon^\pm. \tag{7}$$

B. Equations at leading and first orders, and associated matching conditions

B.1. Matching conditions

The boundary conditions on the metal and at the air/dielectric interface apply for the near field solution (at each order in η). Boundary conditions to be applied to the far field solution, called matching conditions, are written to ensure the continuity of H and C in an intermediate region where the evanescent field can be considered as negligible. It is $y_1 \to \pm\infty$ for the near field solution and it is $x_1 \to 0^{\pm}$ for the far field solution. Owing to the Taylor expansions $H^0(x_1, x_2) = H^0(0, x_2) + x_1 \partial_{x_1} H^0(0, x_2) + \cdots = H^0(0, x_2) + \eta y_1 \partial_{x_1} H^0(0, x_2) + \ldots$ (same for C^0), we get at order 0

$$H^0(0^{\pm}, x_2) = h^0(\pm\infty, y_2, x_2), \quad C^0(0^{\pm}, x_2) = c^0(\pm\infty, y_2, x_2), \tag{8}$$

and at order 1,

$$\begin{cases} H^1(0^{\pm}, x_2) = \lim_{y_1 \to \pm\infty} \left[h^1(y_1) - y_1 \frac{\partial H^0}{\partial x_1}(0^{\pm}, x_2) \right], \\[2mm] C^1(0^{\pm}, x_2) = \lim_{y_1 \to \pm\infty} \left[c^1(y_1) - y_1 \frac{\partial C^0}{\partial x_1}(0^{\pm}, x_2) \right]. \end{cases} \tag{9}$$

B.2. Solution at order 0

In the near field, Eqs. (2) give at leading order, in η^{-1},

$$\nabla_{\mathbf{y}} h^0 = 0, \quad \mathrm{div}_{\mathbf{y}} \mathbf{c}^0 = 0, \tag{10}$$

with the continuities of h^0 and of $\mathbf{c}^0 . \mathbf{n}$ at the air/dielectric interface and $\mathbf{c}^0 . \mathbf{n} = 0$ on the metal. The first equation of the above system tells us that h^0 does not depend on y, and we deduce from the first matching condition in Eqs. (8) that

$$h^0(x_2) = H^0(0^{\pm}, x_2). \tag{11}$$

By integrating over Y the second equation of the Eqs. (10) and owing to (i) $\mathbf{c}^0 . \mathbf{n} = 0$ on the metal ($\partial \mathsf{S}$), (ii) $\mathbf{c}^0 . \mathbf{n}$ continuous at the air/dielectric interface, and (iii) to the periodicity of $\mathbf{c}^0$ w.r.t y_2, we get $\int \mathrm{d}y_2 c_1^0(y_1^m, y_2, x_2) = \int \mathrm{d}y_2 c_1^0(-y_1^m, y_2, x_2)$. Now, we take the limit $y_1^m \to +\infty$, from which the second matching condition in Eqs. (8) gives

$$C_1^0(0^+, x_2) = C_1^0(0^-, x_2), $$

(note that the matching condition has been integrated w.r.t $y_2 \in [0, 1]$). At dominant order, the presence of the metal is not visible: the equivalent interface is simply the interface between the air and the dielectric, with the continuities of H^0 and of C_1^0. To capture the effect of the metallic array, we need to go to the next order.

B.3. Elementary problems

Before going to the next order, unit cell problems are defined, which will make the parameters of the equivalent interface to appear. To that aim, we focus on the problem satisfied by h^1. In the near field, we have

$$\mathbf{c}^0 = \frac{1}{\epsilon(\mathbf{y})} \left[\nabla_{\mathbf{y}} h^1 + \frac{\partial H^0}{\partial x_2}(0, x_2) \mathbf{e}_2 \right]. \tag{12}$$

The above relation is obtained using $\mathbf{C} = 1/\epsilon \nabla H$ written at the order η^0 for the near field solution, and using $h^0(x_2) = H^0(0, x_2)$, Eq. (11). Then, the relation $\mathrm{div}_{\mathbf{y}} \mathbf{c}^0 = 0$ provides a bulk equation for h^1, namely

$$\mathrm{div}_{\mathbf{y}} \left[\frac{1}{\epsilon(\mathbf{y})} \left(\nabla_{\mathbf{y}} h^1 + \frac{\partial H^0}{\partial x_2}(0, x_2) \mathbf{e}_2 \right) \right] = 0, $$

associated to boundary conditions being the continuities of h^1 and of $\mathbf{c}^0 . \mathbf{n}$ at the air/dielectric interface, and $\mathbf{c}^0 . \mathbf{n} = 0$ on the metal. Finally the matching conditions $\mathbf{c}^0(\pm\infty, y_2, x_2) = \mathbf{C}^0(0^{\pm}, x_2)$ give the last boundary conditions needed to solve the problem on h^1 unambiguously. Let us be more specific on these latter conditions. For the far field solution, we have $\mathbf{C}^0(0^{\pm}, x_2) = 1/\epsilon^{\pm} \nabla_{\mathbf{x}} H^0(0^{\pm}, x_2)$, and this tell us that $\partial_{x_1} H^0$ is not continuous at $x_1 = 0$. Using the Eq. (7) in the Eq. (12), the matching conditions read

$$\lim_{y_1 \to \pm\infty} \nabla_{\mathbf{y}} h^1 = \epsilon^{\pm} C_1^0(0, x_2) \mathbf{e}_1. \tag{13}$$

The problem on h^1 appears to be linear w.r.t the quantities $\partial_{x_2} H^0(0, x_2)$ and $C_1^0(0, x_2)$, which will produce significant simplifications. Specifically, let us write

$$h^1(\mathbf{y}, x_2) = C_1^0(0, x_2) h^{(1)}(\mathbf{y}) + \frac{\partial H^0}{\partial x_2}(0, x_2) h^{(2)}(\mathbf{y}). \tag{14}$$

It is easy to see that h^1 is solution of the problem if $h^{(1)}$ satisfies

$$\begin{cases} \mathrm{div} \left[\frac{1}{\epsilon(\mathbf{y})} \nabla h^{(1)} \right] = 0, \\[2mm] \lim_{y_1 \to \pm\infty} \nabla h^{(1)} = \epsilon^{\pm} \mathbf{e}_1, \end{cases} \tag{15}$$

with $h^{(1)}$ and $1/\epsilon(\mathbf{y})\boldsymbol{\nabla} h^{(1)}.\mathbf{n}$ being continuous at the air/dielectric interface and $\boldsymbol{\nabla} h^{(1)}.\mathbf{n} = 0$ on the metal, and if $h^{(2)}$ satisfies

$$\begin{cases} \operatorname{div}\left[\dfrac{1}{\epsilon(\mathbf{y})}\boldsymbol{\nabla}(h^{(2)} + y_2)\right] = 0, \\[3mm] \lim_{y_1 \to \pm\infty} \boldsymbol{\nabla} h^{(2)} = \mathbf{0}, \end{cases} \tag{16}$$

with the same boundary conditions as $h^{(1)}$. $(h^{(1)}, h^{(2)})$ are of the form

$$h^{(1)} = \begin{cases} \epsilon^- y_1 + h_{ev}^{(1)}, \\[2mm] \epsilon^+ y_1 + \mathcal{B} + h_{ev}^{(1)}, \end{cases} \qquad h^{(2)} = \begin{cases} h_{ev}^{(2)}, & y_1 < 0, \\[2mm] \mathcal{B}' + h_{ev}^{(2)}, & y_1 > 0. \end{cases} \tag{17}$$

where $(h_{ev}^{(1)}, h_{ev}^{(2)})$ are evanescent fields. The evanescent fields, as the constant $(\mathcal{B}, \mathcal{B}')$, depend on the shape of the metallic array and on ϵ_r. Except in some particular cases, that will be considered in the following, the problems have to be solved numerically; we will see in the following section that these unit cell problems define the interface parameters.

B.4. Solution at order 1

The jump of H^1 directly follows from the first matching condition in Eqs. (9), using Eq. (14), with Eqs. (17)

$$\left[\!\left[H^1 \right]\!\right] = \mathcal{B} C_1^0(0, x_2) + \mathcal{B}' \frac{\partial H^0}{\partial x_2}(0, x_2). \tag{18}$$

To determine the jump in C_1^1, we integrate over Y the first equation of Eqs. (2) written for the near field solution at order 0 in η

$$\operatorname{div}_{\mathbf{y}}\mathbf{c}^1 + \frac{\partial c_2^0}{\partial x_2} + H^0(0, x_2) = 0. \tag{19}$$

Next, we use, in $\mathsf{Y}^\pm$, the relations $1/\epsilon^\pm \, \partial_{x_2}^2 H^0 + H^0 = -1/\epsilon^\pm \partial_{x_1}^2 H^0 = -\partial_{x_1} C_1^0$. With $\mathbf{c}^0$ given in Eq. (12), the integration of Eq. (19) over Y reads

$$\int_{\mathsf{Y}} d\mathbf{y} \, \operatorname{div}_{\mathbf{y}}\mathbf{c}^1 + \frac{\partial}{\partial x_2} \int_{\mathsf{Y}} \frac{d\mathbf{y}}{\epsilon(\mathbf{y})} \frac{\partial h^1}{\partial y_2} - \int_{\mathsf{Y}^+} d\mathbf{y} \, \frac{\partial C_1^0}{\partial x_1}(0^+, x_2) - \int_{\mathsf{Y}^-} d\mathbf{y} \, \frac{\partial C_1^0}{\partial x_1}(0^-, x_2) = 0.$$

Because $\mathbf{c}^1.\mathbf{n}$ is continuous at the air/dielectric interface and vanishes on the metal, and because $\mathbf{c}^1$ is periodic *w.r.t* y_2, the first integral of the above equation reduces to $\int d\mathbf{y}' \; [c_1^1(y_1^m, y_2, x_2) - c_1^1(-y_1^m, y_2, x_2)]$. The two last integrals are respectively equal to $-y_1^m \partial_{x_1} C_1^0(0^+, x_2)$ and $-(y_1^m - \mathcal{S})\partial_{x_1} C_1^0(0^-, x_2)$ because of the disymmetry in $\mathsf{Y}^\pm$. Finally, using the matching condition, Eq. (9) and Eq. (14), we get for $y_1^m \to +\infty$,

$$\left[\!\left[C_1^1 \right]\!\right] = \mathcal{D} \frac{\partial C_1^0}{\partial x_2}(0, x_2) + \mathcal{C} \frac{\partial^2 H^0}{\partial x_2^2}(0, x_2) - \mathcal{S} \frac{\partial C_1^0}{\partial x_1}(0^-, x_2),$$

with

$$\mathcal{D} \equiv -\int_{\mathsf{Y}} \frac{d\mathbf{y}}{\epsilon(\mathbf{y})} \frac{\partial h^{(1)}}{\partial y_2}(\mathbf{y}), \quad \mathcal{C} \equiv -\int_{\mathsf{Y}} \frac{d\mathbf{y}}{\epsilon(\mathbf{y})} \frac{\partial h^{(2)}}{\partial y_2}(\mathbf{y}). \tag{20}$$

B.5. Final jump conditions and interface parameters

To express the final jump conditions, we use that $\left[\!\left[H \right]\!\right] = \eta \left[\!\left[H^1 \right]\!\right] + O(\eta^2)$ (same for C_1^1) and $H = H^0 + O(\eta)$. It is now sufficient to come back to the real space $H(\mathbf{X}) = H(\mathbf{x})$ with $\partial_{X_i} = k\partial_{x_i}$ to get the jump conditions

$$\begin{cases} \left[\!\left[H \right]\!\right] = h\mathcal{B}\overline{C_1} + h\mathcal{B}' \overline{\dfrac{\partial H}{\partial X_2}}, \\[4mm] \left[\!\left[C_1 \right]\!\right] = \quad h\mathcal{D}\overline{\dfrac{\partial C_1}{\partial X_2}} + h\mathcal{C}\overline{\dfrac{\partial^2 H}{\partial X_2^2}} - h\mathcal{S}\dfrac{\partial C_1}{\partial X_1}(0^-, X_2), \end{cases} \tag{21}$$

and the second jump condition is equivalent to a jump in E_2 through the Eq. (3). It can be noticed that now, the right hand side terms involve values of the fields at both sides of an interface with zero thickness. For this interface, the thickness e has not really disappear, being encapsulated in the interface parameters. Nevertheless, it is useful to restore this small but finite thickness in the jump conditions. This is done by "enlarging" the equivalent interface; to do that, we define $H^+ = H(0^+, X_2)$ and $H^- = H(-e, X_2)$ (with the convention of $X_1 = 0$ in Fig. 1). At dominant order, this does not affect the right hand side terms in Eqs. (21), namely $\overline{C_1} = 1/2(C_1^+ + C_1^-) + O(e)$. Next, we define new jump conditions $\left[\!\left[C_1 \right]\!\right]_e \equiv C_1^+ - C_1^- = \left[\!\left[C_1 \right]\!\right] + e\partial_{X_1} C_1^- + O(e^2)$, where we have used a Taylor expansion of $C_1(-e)$. The jump conditions at the new equivalent interface of thickness e finally read

$$\begin{cases} \left[\!\left[H \right]\!\right]_e = \left(\dfrac{h\mathcal{B}}{2} + \epsilon^- e\right) C_1^- + \dfrac{h\mathcal{B}}{2} C_1^+ + \dfrac{h\mathcal{B}'}{2}\left[\dfrac{\partial H^-}{\partial X_2} + \dfrac{\partial H^+}{\partial X_2}\right], \\[4mm] \left[\!\left[C_1 \right]\!\right]_e = \quad \dfrac{h\mathcal{D}}{2}\left[\dfrac{\partial C_1^-}{\partial X_2} + \dfrac{\partial C_1^+}{\partial X_2}\right] + \dfrac{h\mathcal{C}}{2}\left[\dfrac{\partial^2 H^-}{\partial X_2^2} + \dfrac{\partial^2 H^+}{\partial X_2^2}\right] + (e - h\mathcal{S})\dfrac{\partial C_1^-}{\partial X_1}. \end{cases} \tag{22}$$

3. NUMERICAL VALIDATION

In order to validate our homogenization approach, and to compare with results coming from the transmission line theory, we consider a metallic array composed of strips (Fig. 3). Significant simplifications occur in the jump conditions, Eqs. (22). This is because $h^{(1)}$ is symmetric with respect to y_2, see Eqs. (15), leading to $\mathcal{D} = 0$ in Eq. (20); also, $h^{(2)}$ is antisymmetric with respect to y_2, from which $\mathcal{B}' = 0$. Thus, the interface parameters reduce to $(\mathcal{B}, \mathcal{C}, \mathcal{S})$ among which the dimensionless surface of the metallic array $\mathcal{S}$, for a plate $\mathcal{S} = e\ell/h^2$. Also, $\mathcal{B}$ is known and a good estimate of $\mathcal{C}$ is obtained (see the Appendix A)

$$
\begin{cases}
\mathcal{B} = e\dfrac{\ell}{h-\ell} - \dfrac{\epsilon_r + 1}{\pi} \log\left(\sin\dfrac{\pi}{2}\left(1-\dfrac{\ell}{h}\right)\right), \\
\mathcal{C} \simeq \dfrac{e}{h}\left(1 - \dfrac{\ell}{h}\right) - \dfrac{\pi}{8}\left(1 - \dfrac{\ell}{h}\right)^2, \quad \text{for } e > h(1-\ell),
\end{cases}
\tag{23}
$$

and $\mathcal{C}$ can be neglected for $e < h(1-\ell)$. Owing to $\epsilon^- = 1, \epsilon^+ = \epsilon_r$, the jump conditions Eqs. (22) can be written in terms of H and its spatial derivatives. Specifically, we have

$$
\begin{cases}
H^+ - H^- = \left(\dfrac{h\mathcal{B}}{2} + e\right)\dfrac{\partial H^-}{\partial X_1} + \dfrac{h\mathcal{B}}{2\epsilon_r}\dfrac{\partial H^+}{\partial X_1}, \\
\dfrac{1}{\epsilon_r}\dfrac{\partial H^+}{\partial X_1} - \dfrac{\partial H^-}{\partial X_1} = \dfrac{h\mathcal{C}}{2}\left[\dfrac{\partial^2 H^-}{\partial X_2^2} + \dfrac{\partial^2 H^+}{\partial X_2^2}\right] + (e - h\mathcal{S})\dfrac{\partial^2 H^-}{\partial X_1^2}.
\end{cases}
\tag{24}
$$

A. Scattering coefficients

The scattering problem for the real structure is shown in Fig. 3. A plane wave hits the metallic array at incidence θ in the (X_1, X_2) plane, with $\mathbf{k}^{\text{inc}} = k(\cos\theta, \sin\theta)$ (and $\mathbf{H}^{\text{inc}}$ is along $\mathbf{e}_3$). The metallic array, of thickness e, is located at a distance d from the metallic ground plane, in $-e \leq X_1 \leq 0$; finally the dielectric material occupies $0 \leq X_1 \leq d$. This problem is solved numerically using full wave simulations based on a multimodal method [20, 21]. In the numerics, the resolution is done on the magnetic field $H(X_1, X_2)$, and we get the reflection coefficient $R = -H^r/H^{\text{inc}}$ (H^{inc} and H^r refer to the incident and reflected fields at $X_1 = 0$).
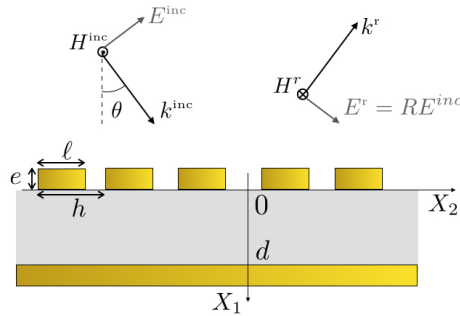

Fig. 3. The scattering problem for the whole metasurface. The reflection coefficient $R = -H^r/H^{\text{inc}}$ is obtained numerically. In the homogenized problem, the metallic array is replaced by the equivalent interface and the propagation in the dielectric slab is explicitly solved.

This coefficient R refers to the Fresnel reflection coefficient of the electric field for the conventions in the orientations of the fields shown in Fig. 3. With these conventions, the components of the electric field are $E_1(0, X_2) = \sin\theta(R-1)E^{\text{inc}}e^{-ik\sin\theta X_2}$, $E_2 = \cos\theta(R+1)E^{\text{inc}}e^{-ik\sin\theta X_2}$. Next, with $H(X_1 < -e, X_2)$ in the free space written in the form

$$
H(X_1, X_2) = \left[H^{\text{inc}}e^{-ik\cos\theta X_1} + H^r e^{ik\cos\theta X_1}\right]e^{-ik\sin\theta X_2},
$$

and using Eqs.(3), we get $H^r/H^{\text{inc}} = -R$ (and $E^{\text{inc}} = \sqrt{\mu_0/\epsilon_0}H^{\text{inc}}$).

B. The scattering coefficients in the homogenized problem

In the homogenized problem, the metallic array is replaced by the equivalent interface. Thus, the solution is of the form

$$
H(X_1, X_2) = \begin{cases}
\left[e^{-ik\cos\theta X_1} - R_h e^{ik\cos\theta X_1}\right]e^{-ik\sin\theta X_2}, & X_1 < -e, \\
B\cos K(X_1 - d)e^{-ik\sin\theta X_2}, & d \geq X_1 > 0,
\end{cases}
\tag{25}
$$

with $K \equiv k\sqrt{\epsilon_r - \sin^2 \theta}$ the component along X_1 of the wavenumber in the dielectric (and R_h stands for the reflection coefficient of the homogenized solution). Applying the jump conditions Eqs. (24), the reflection coefficient R_h is easily obtained

$$\begin{cases} R_h = & -e^{2ik\cos\theta e}\dfrac{Z_h}{Z_h{}^*}, \\[2mm] Z_h = & \left[i + k\cos\theta\left(\dfrac{\mathcal{B}h}{2} + e\right)\right]\left[\dfrac{K}{\epsilon_r}\tan Kd + \dfrac{\mathcal{C}h}{2}k^2\sin^2\theta\right] \\[2mm] & -k\cos\theta\left[1 - ik\cos\theta\left(e - \mathcal{S}h + \dfrac{\mathcal{C}h}{2}\tan^2\theta\right)\right]\left[1 - \dfrac{\mathcal{B}h}{2\epsilon_r}K\tan Kd\right], \end{cases} \tag{26}$$

with $Z_h{}^*$ the complex conjugate of Z_h. As expected, R_h is of modulus unity.

C. The case $e = 0$, comparison with the transmission line theory

One powerful method to describe the scattering properties of dielectric-metal structures is the transmission line theory [22]. It is based on the identification of an electric circuit characterized by an equivalent input impedance. Generally speaking, once all the components of the device have been identified and associated to impedances being placed in parallel or in series, the input impedance is obtained, from which the scattering properties are deduced. Nevertheless, the method is restricted to simple geometries of the metallic parts with zero thickness, being of capacitive type (large plates separated by small gaps) or inductive type (small metal strips with large air gaps). The device of Fig. 1 has been studied in [16] for an electric field being polarized along $\mathbf{e}_2$, and the denomination TM is used for this configuration in this reference; the metallic plates are of capacitive type in this case (the other polarization considered in [16], with the electric field along $\mathbf{e}_3$, is discussed in the Appendix B). In our study, TM refers to a magnetic field being polarized along $\mathbf{e}_3$, and thus, the two approaches can be compared for normal incident wave only. The calculation presented in this paper ends with the expression of R of the form

$$R^{TL} = -\frac{1 - Z/Z_0}{1 + Z/Z_0},$$

where Z/Z_0 is given by

$$Z/Z_0 = i\,\frac{\tan Kd/\sqrt{\epsilon_r}}{1 - kh\mathcal{B}_0\tan Kd(\epsilon_r + 1)/\sqrt{\epsilon_r}},$$

with

$$\mathcal{B}_0 = -\frac{1}{\pi}\log\left(\sin\frac{\pi}{2}\left(1 - \frac{\ell}{h}\right)\right),$$

(we have used the Eqs. (13) and (20) in Ref. [16] for $\theta = 0$). In [16], the coefficient $\mathcal{B}_0$ appears through the so-called grid parameter $\alpha = kh\mathcal{B}_0$, with k being replaced heuristically by an averaged wavenumber $k_{eff} = k\sqrt{(\epsilon_r + 1)/2}$. The coefficient $\mathcal{B}_0$ is known in fluid mechanics for potential flows around a flat plate; it corresponds to the problem whose solution is $h^{(1)}$ for $\epsilon_r = 1$, and it is called the blockage coefficient in this context [23].

For $e = 0$, our interface parameters simplify, with obviously $\mathcal{S} = 0$ and from Eqs. (23), $\mathcal{B} = (1 + \epsilon_r)\mathcal{B}_0$ and $\mathcal{C} = 0$. At normal incidence $\theta = 0$, we get from Eq. (26)

$$Z_h^{e=0} = -k\left[1 - \frac{\mathcal{B}h}{\epsilon_r}K\tan Kd\right] + i\frac{K}{\epsilon_r}\tan Kd.$$

It is easy to see that $Z_h^{e=0} = C(1 - Z/Z_0)$ (and $C = -k\left[1 - \mathcal{B}hK\tan Kd/\epsilon_r\right]$ is purely real). With Z/Z_0 purely imaginary, $Z_h{}^* = C(1 + Z/Z_0)$. Thus both approaches give the same result in this limiting case $\theta = 0$.

D. Numerical validation of the reflection phase

In this section, we inspect the validity of our prediction, Eq. (26), on the reflection phase. We consider a metallic array with $h = 2$ mm, $\ell = 1.8$ mm; otherwise, $\epsilon_r = 10$ and $d = 1$ mm.

Fig. 4 reports the variations of the reflection phase as a function of the frequency for vanishing thickness of the metal, $e \simeq 0$, (in the numerics, $e = 10^{-3}$ mm has been considered), and $\theta = 0, 60$ and $85°$. The dotted line in Fig. 4 shows the reflection phase due to the dielectric slab only (for normal incidence). It is visible that the metallization allows for higher variations in the reflection phase, as expected. For $e = 0$, the in-plane reflection is obtained at the low central frequency of 11.75 GHz, with a useful bandwidth of 2.5 GHz (frequency range [10.5-13] GHz realizing the transition from $90°$ to $-90°$). The plain lines show the reflection phase in the homogenized problem, R_h in Eq. (26) (with $\mathcal{S} = \mathcal{C} = 0$ and $\mathcal{B} = 6.49$ from Eq. (23)). The agreement between direct numerics and homogenization is very good, about 1%, for the 3 incidences considered. In this case, the parameter $\eta = kh$ ranges in [0.25; 0.75] for frequencies in [6, 18] GHz; this is reasonable since $\eta < 1$, but it can be noticed that the homogenization is not restricted to very small η-values.

Next, we inspect the influence of the thickness e of the metallic array. Figs. 5 report the variations of the reflection phase for $e = 0, 1$ and 2 mm ($\theta = 0$ and $60°$ have been considered). The sensitivity to the thickness is visible: when e increases, the central frequency of the in-phase reflection is shifted significantly, from 11.75 GHz to 9.5 and 8 GHz at normal incidence (for $e = 1$ and 2 mm respectively); note that the useful bandwidths decrease slightly, but not significantly, and they remain close to 2 GHz. Next varying e makes $\mathcal{B}$ to increase, Eq. (23), and thus, produces a decrease in the frequency realizing the in phase reflection. As in Fig. 4, we reported in Fig. 5 the reflection phase of R_h in the homogenized problem in plain lines. For $e = 1$ mm, we find $\mathcal{B} = 11.0$, $\mathcal{C} = 0.048$ (and $\mathcal{S} = 0.45$); for $e = 2$ mm, we find $\mathcal{B} = 15.50$, $\mathcal{C} = 0.098$ (and $\mathcal{S} = 0.9$). Here, we still have $\eta = kh < 0.75$, with ke up to 0.4 for $e = 1$ mm and ke up to 0.8 for $e = 2$ mm. The agreement with the homogenized result remains very good but slightly decreases when e increases, from 1-2% for $e \simeq 0$, to 3-4% for $e = 1$ mm and to 5-7% for $e = 2$ mm.
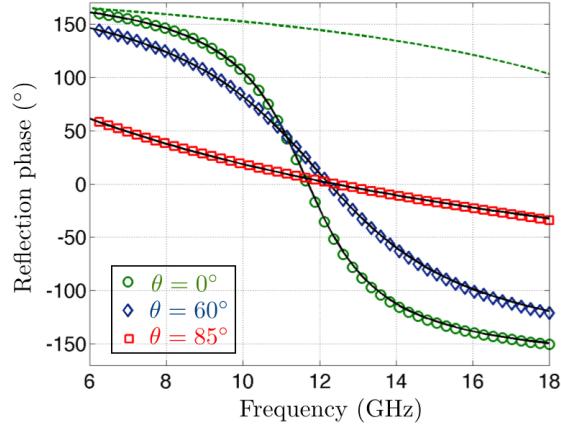
Fig. 4. Reflection phase diagram. The parameters of the AMC structure are $h = 2$ mm, $\ell = 1.8$ mm, $d = 1$ mm, $e \simeq 0$ and $\epsilon_r = 10$. Symbols correspond to full numerics and plain lines to the homogenized results, R_h in Eq. (26). The dotted line shows the reflection phase due to the dielectric slab in the absence of metallization (for $\theta = 0$).
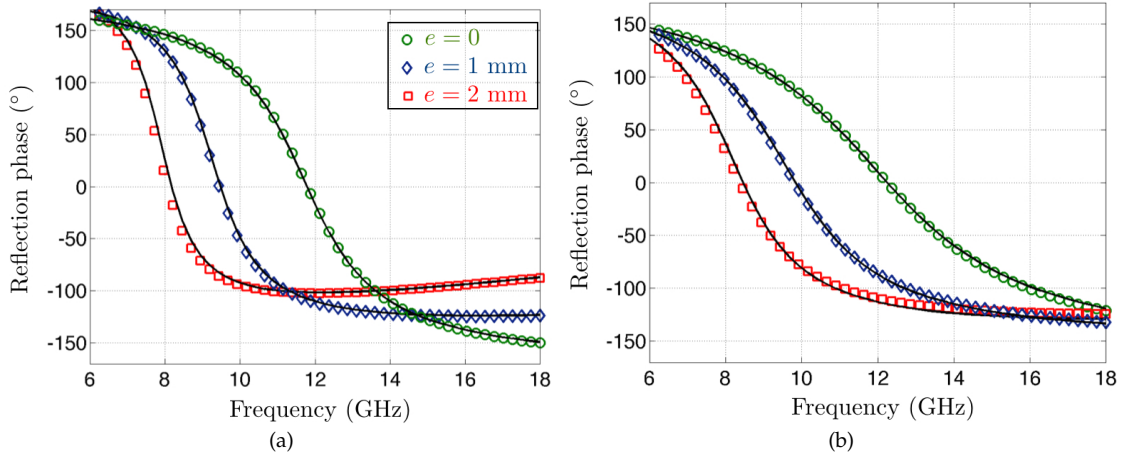

Fig. 5. Reflection phase diagram for (a) $\theta = 0$ and (b) $\theta = 60°$. The parameters of the AMC structure are $h = 2$ mm, $\ell = 1.8$ mm, $d = 1$ mm, $\epsilon_r = 10$ and $e = 0$, 1 mm or 2 mm. Symbols correspond to full numerics and plain lines to the homogenized results, R_h in Eq. (26).

E. Numerical validation of the guided waves

The ability of metamaterial surfaces to modify the band structure of guided waves has practical applications, notably to improve the directivity of printed antenna (in this case, surface wave propagation is unwanted). In [16], the band structure of guided waves was inspected for $e = 0$. In this section, we generalize the dispersion relation to non vanishing e and we show that an increase in e increases the band gap, resulting also in a decrease in the wavelength of the guided wave. Guided waves are solution of the homogeneous problem in the absence of a source or of an incident wave. Thus, they are of the form

$$H(X_1, X_2) = \begin{cases} e^{\alpha(X_1+e)}e^{-i\beta X_2}, & X_1 < -e, \\ \\ B \cos K(X_1 - d)e^{-i\beta X_2}, & d \geq X_1 > 0, \end{cases}$$

with $\alpha = \sqrt{\beta^2 - k^2}$, $K = \sqrt{\epsilon_r k^2 - \beta^2}$ (and $k < \beta$). Applying the boundary condition, Eqs. (24), the dispersion relation of the guided wave reads

$$\left[\frac{K}{\epsilon_r} \tan Kd + \frac{\mathcal{C}h}{2}\beta^2 \right] \left[1 + \left(\frac{\mathcal{B}h}{2} + e \right)\alpha \right] - \left[1 - \frac{\mathcal{B}h}{2\epsilon_r}K \tan Kd \right] \left[\alpha - \frac{\mathcal{C}h}{2}\beta^2 + (e - \mathcal{S})\alpha^2 \right] = 0. \tag{27}$$

In the limit of zero thickness array, it simplifies to

$$\sqrt{\beta^2 - k^2}\left[1 - h\mathcal{B}_0 K \tan Kd \left(1 + 1/\epsilon_r \right) \right] = \frac{K}{\epsilon_r} \tan Kd,$$

from which it is clear that the metallization reinforces the confinement of the wave guided within the dielectric slab, obtained setting $\mathcal{B}_0$ to zero in the above relation (namely, in the absence of the metallization, the dispersion relation reduces to $\sqrt{\beta^2 - k^2} = K \tan Kd/\epsilon_r$).

Now, we inspect the effect of increasing the array thickness, and the ability of our interface conditions to capture this effect. The Fig. 6 reports the dispersion relations of the guided waves for $h = 2$ mm, $\ell = 0.8$ mm, $d = 4$ mm, and we have considered $e \simeq 0$ and $e = 4$ mm. For comparison, the dispersion relation of the structure without the metallic array is shown in dash-dot line.
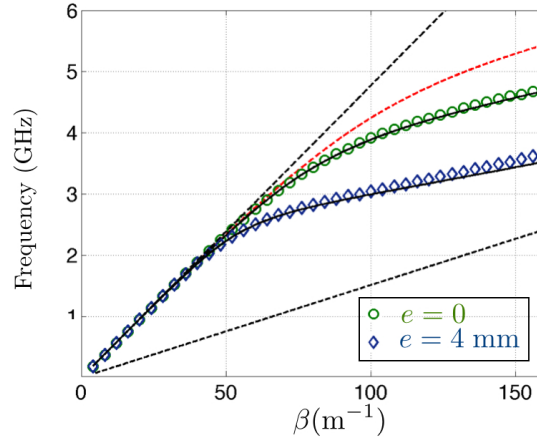

Fig. 6. Dispersion relation of the wave guided by the metasurface, with wavelength $2\pi/\beta$. The parameters are $h = 2$ mm, $\ell = 1.8$ mm, $d = 4$ mm, $\epsilon_r = 10$; $e \simeq 0$ and $e = 4$ mm are considered. Symbols correspond to full numerics and plain lines to the homogenized results, Eq. (27). The two dotted lines show the light lines of the air $\beta = k$ and of the dielectric $\beta = \epsilon_r k$. The dash-dot line shows the dispersion relation for the dielectric slab alone (without any metallization).

It is visible that non zero thicknesses of the metal affect the band structure of the guided waves. Specifically, an increase in e enlarges the band gap. The homogenized prediction (plain lines) is obtained by solving the dispersion relation, Eq. (27), where the dependance in e is encapsulated in the interface parameters $(\mathcal{S}, \mathcal{B}, \mathcal{C})$. The agreement is very good for $e \simeq 0$ (0.7%) and increases, as expected, for $e = 4$ mm (2%); in the present geometry, we have $kh < 0.2$ and $ke < 0.33$. Beyond the observed agreement, it is visible that the wavelength of the guided wave decreases when e increases, a fact that could be used for practical applications. This change in the wavelength of the guided waves is exemplified in Fig. 7, where we reported the magnetic fields $H(X_1, X_2)$ of the guided waves at 3.5 GHz, for $e \simeq 0$ and $e = 4$ mm. At this frequency, the guided wave for the dielectric alone (without any metallization) would have roughly the same characteristics as the one in Fig. 7(a). The resulting wavelengths $2\pi/\beta$ are 74 mm ($\beta = 85$ m^{-1}) and 40 mm ($\beta = 153$ m^{-1}) respectively.
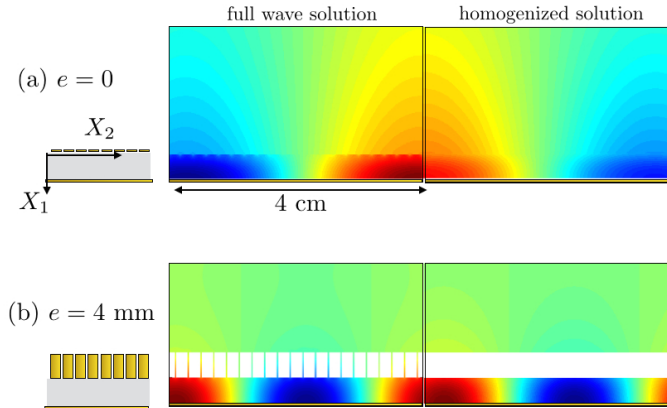

Fig. 7. Two dimensional magnetic wavefields $H(X_1, X_2)$ of the guided wave. (a) for $e = 0$ and (b) for $e = 4$ mm, the parameters are the same as in Fig. 6.

4. CONCLUSION

We have presented a homogenization model able to describe the properties of metasurfaces made of thin metallo-dielectric structure by jump conditions at an equivalent interface. We have exemplified the accuracy of the method in the case of simple rectangular plates of metal. The model accurately describes the variations of the reflection phase in the low frequency regime, namely for $ke, kh < 1$ as the band structure of the guided waves. While the limiting case of vanishing thickness $e \simeq 0$ recovers the prediction given by transmission line theory, we have illustrated the effect of small but finite metallization thicknesses. Natural extensions of the present study concerns more involved repartitions of the metallization, notably non symmetric repartitions of metal in the unit cell which

are able to make hybridization to appear. Except in particular configurations, extensions to three dimensional geometries require the whole Maxwell equations to be considered, in order to allow for changes in the wave polarization. Finally, these metasurfaces, say of AMC-type, involve resonances in the dielectric substrate, being reduced to subwavelength scale by the metallization. Other metasurfaces involve resonances of components within the unit cell; in this case, the presented homogenization can be adapted which would make frequency dependent effective parameters to appear.

ACKNOWLEDGMENTS

A. THE INTERFACE PARAMETERS

The Figs. 8 report the variations of $\mathcal{B}$ and $\mathcal{C}$ as a function of ℓ/h for different e-values. They have been calculated by means of the resolution of the unit cell problems, Eqs. (15)-(16); we have considered $\epsilon_r = 10$ in these calculations. Inspecting further the influence of the ϵ_r value, we found that $\mathcal{B}$ behaves accordingly to Eq. (23) with the accuracy of the numerical resolution. The approximation given in Eqs. (23) for $\mathcal{C}$ is rather satisfactory, with less than 1% for $\epsilon_r = 1$ and 5% for $\epsilon_r = 10$.
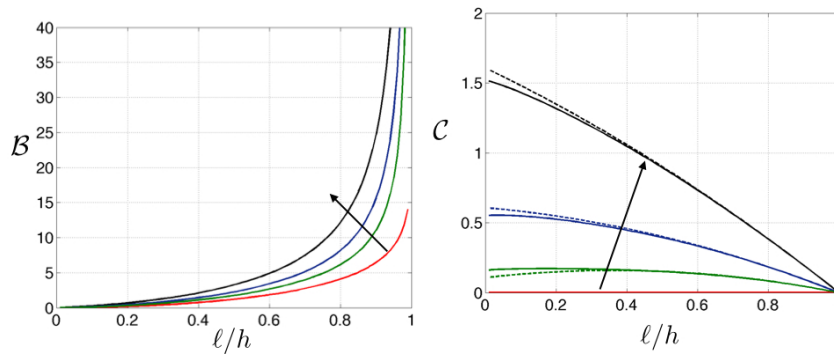

Fig. 8. Variations of $\mathcal{B}$ and $\mathcal{C}$ with ℓ/h; the arrows indicate increasing values of e/h ($e/h = 0, 0.5, 1$ and 2). $\epsilon_r = 10$ has been considered. Plain lines show the results coming from the resolution of the elementary problems and dotted lines the predictions in Eqs. (23).

B. THE CASE OF TRANSVERSE ELECTRIC POLARIZATION

Transverse electric polarization corresponds to an electric field being polarized along $\mathbf{e}_3$ in Fig. 1. In this case, the Helmholtz equation applied for $\mathbf{E}(\mathbf{X}) = E(\mathbf{X})\mathbf{e}_3$ leading to the problem

$$\text{div}\left[\boldsymbol{\nabla} E\right] + \epsilon k^2 E = 0, \tag{28}$$

and, as previously, ϵ depends on space. The boundary conditions between the air and the dielectric are the continuities of E and of $\boldsymbol{\nabla} E.\mathbf{n}$ and the boundary condition on the metal is $E = 0$. As in the TM polarization, we define an auxiliary field $\mathbf{G}$, with $\boldsymbol{\nabla} E = k\mathbf{G}$, so that the Eq. (28) reads

$$\text{div}\mathbf{G} + \epsilon k E = 0, \quad \mathbf{G} \equiv \frac{1}{k}\boldsymbol{\nabla} E, \tag{29}$$

with boundary conditions being the continuity of $\mathbf{G}.\mathbf{n}$ at the air/dielectric interface, and $E = 0$ on the metal.

A. Homogenization for TE polarization

In the far field, we use

$$E = E^0(\mathbf{x}) + \eta E^1(\mathbf{x}) + \dots,$$
$$\mathbf{G} = \mathbf{G}^0(\mathbf{x}) + \eta \mathbf{G}^1(\mathbf{x}) + \dots, \tag{30}$$

and in the near field

$$E = e^0(\mathbf{y}, x_2) + \eta e^1(\mathbf{y}, x_2) + \dots,$$
$$\mathbf{G} = g^0(\mathbf{y}, x_2) + \eta g^1(\mathbf{y}, x_2) \dots. \tag{31}$$

Finally, the matching conditions on $(E^n, \mathbf{G}^n)$ and (e^n, g^n), $n = 0, 1$, are as in Eqs. (8)-(9), owing to $H \to E$ and $\mathcal{C} \to \mathbf{G}$. Now, the Eq. (29) will be inspected at leading and first orders in η using the differential operators, Eqs. (6).

At leading order (η^{-1}), we have, from the second equation in Eqs. (29), $\nabla_{\mathbf{y}} e^0 = 0$, from which $e^0(x_2)$ is independent of $\mathbf{y}$. Because the boundary condition $e^0 = 0$ is written in terms of the spatial coordinates $\mathbf{y}$, we deduce that $e^0(x_2) = 0$ everywhere, and with the matching condition, we get

$$e^0(x_2) = E^0(0, x_2) = 0, \quad \frac{\partial E^0}{\partial x_2}(0, x_2) = 0, \tag{32}$$

(and the latter equation is a consequence of the former). Note that the result is very different from the TM case: here, we have at leading order a boundary condition on E^0 rather than a jump condition. Besides, we found that the metallic array was invisible at leading order in the TM case, and only the air/dielectric interface conditions was visible. Here to the contrary, we find that only the metal is visible. To capture the effect of the array structuration and to restore the air/dielectric interface, we need to inspect the behavior of E^1. The first equation in Eqs. (29) gives, at order η^{-1}: $\mathrm{div}_{\mathbf{y}} g^0 = 0$, and the second at order η^0: $g^0 = \nabla_{\mathbf{y}} e^1$ (using that $de^0/dx_2 = 0$, from Eq. (32)). It follows that e^1 is solution of

$$\begin{cases} \Delta_y e^1 = 0, \\ \lim_{y_1 \to \pm\infty} \nabla_{\mathbf{y}} e^1 = \frac{\partial E^0}{\partial x_1}(0^{\pm}, x_2)\mathbf{e}_1, \end{cases} \tag{33}$$

with $e^1 = 0$ on the metallic array. By linearity of the above system, we can use

$$e^1(\mathbf{y}, x_2) = \frac{\partial E^0}{\partial x_1}(0^+, x_2)e^+(\mathbf{y}) + \frac{\partial E^0}{\partial x_1}(0^-, x_2)e^-(\mathbf{y}), \tag{34}$$

and e^1 is solution of Eqs. (33) as soon as $\mathbf{e}^{\pm}$ are solutions of

$$\begin{cases} \Delta e^{\pm} = 0, \\ \lim_{y_1 \to -\infty} \nabla e^+ = \mathbf{0}, \quad \lim_{y_1 \to +\infty} \nabla e^+ = \mathbf{e}_1, \\ \lim_{y_1 \to -\infty} \nabla e^- = \mathbf{e}_1, \quad \lim_{y_1 \to +\infty} \nabla e^- = \mathbf{0}, \end{cases}$$

with $e^{\pm} = 0$ on the metallic array. The solutions $e^{\pm}$ are of the form

$$e^+ = \begin{cases} \mathcal{A}_1^+ + e_{\mathrm{ev}}^+, & y_1 < 0, \\ \mathcal{A}_2^+ + y_1 + e_{\mathrm{ev}}^+, & y_1 \geq 0, \end{cases}$$

$$e^- = \begin{cases} \mathcal{A}_2^- + y_1 + e_{\mathrm{ev}}^-, & y_1 < 0, \\ \mathcal{A}_1^- + e_{\mathrm{ev}}^-, & y_1 \geq 0, \end{cases} \tag{35}$$

where $e_{\mathrm{ev}}^{\pm}(\mathbf{y})$ are evanescent fields, and it is easy to see that $\mathcal{A}_1 \equiv \mathcal{A}_1^+ = -\mathcal{A}_1^-$ (looking for $\int d\mathbf{y}\, e^{\pm} \Delta e^{\mp} = 0$). Besides, for inclusions being symmetric w.r.t $\mathcal{A}_2 = \mathcal{A}_2^+ = e/h - \mathcal{A}_2^-$.

It si now sufficient to use the matching condition on $E^1(0^{\pm}, x_2) = \lim_{y_1 \to \pm\infty}\left[e^1 - y_1 \partial_{x_1} E^0(0^{\pm}, x_2)\right]$ to find the boundary conditions expressed in the real space

$$\begin{cases} E(0^-, X_2) = (e - h\mathcal{A}_2)\frac{\partial E}{\partial X_1}(0^-, X_2) + h\mathcal{A}_1\frac{\partial E}{\partial X_1}(0^+, X_2), \\ E(0^+, X_2) = -h\mathcal{A}_1\frac{\partial E}{\partial X_1}(0^-, X_2) + h\mathcal{A}_2\frac{\partial E}{\partial X_1}(0^+, X_2). \end{cases}$$

Finally, using $E^+ = E(0^+)$ and $E^- = E(-e)$ to restore the small but finite thickness of the array, we get

$$\begin{cases} E^- = -h\mathcal{A}_2\frac{\partial E^-}{\partial X_1} + h\mathcal{A}_1\frac{\partial E^+}{\partial X_1}, \\ E^+ = -h\mathcal{A}_1\frac{\partial E^-}{\partial X_1} + h\mathcal{A}_2\frac{\partial E^+}{\partial X_1}. \end{cases} \tag{36}$$

B. The scattering problem in TE polarization

For a wave at oblique incidence on the structure, the solution is thought as in Eq. (25)

$$E(X_1, X_2) = \begin{cases} \left[e^{-ik\cos\theta X_1} + R_h e^{ik\cos\theta X_1}\right]e^{-ik\sin\theta X_2}, & X_1 \leq -e, \\ \\ B\sin K(X_1 - d)e^{-ik\sin\theta X_2}, & d \geq X_1 \leq 0, \end{cases}$$

with $K \equiv k\sqrt{\epsilon_r - \sin^2\theta}$ the component along X_1 of the wavenumber in the dielectric (as previously, R_h stands for the reflection coefficient of the homogenized solution). At the equivalent interface, applying the jump conditions, Eqs. (37), we get

$$
\begin{cases}
R_h = & -e^{2ik\cos\theta e}\dfrac{Z_h}{Z_h{}^*}, \\[2mm]
Z_h = & [1 - ikh\mathcal{A}_2\cos\theta]\left[\tan Kd + \mathcal{A}_2 Kh\right] + i\mathcal{A}_1^2 kKh^2\cos\theta.
\end{cases}
\tag{37}
$$

However, it is easy to check that the presence of the array in this polarization has no particular interest in term of the control of the reflection phase. Indeed, for small device (say, d/e of order unity), even with very sparse metallic parts ($\ell, e \ll h$), the Dirichlet condition is dominant and tends to impose a constant phase, close to $180°$ (in fact, the variation of the reflection phase in the absence of the array are more significant). This was not the case in TM polarization, see Fig. 4.

C. The interface parameters in TE and the case $e = 0$

We report in Fig. 9 the variations of $(\mathcal{A}_1, \mathcal{A}_2)$ with ℓ/h for $e/h = 0, 1$. Because the unit cell problems do not depend on ϵ_r, the interface parameters are unaffected by a change in the permittivity of the dielectric (they would be affected by a change in the permeability, which has been disregarded here).
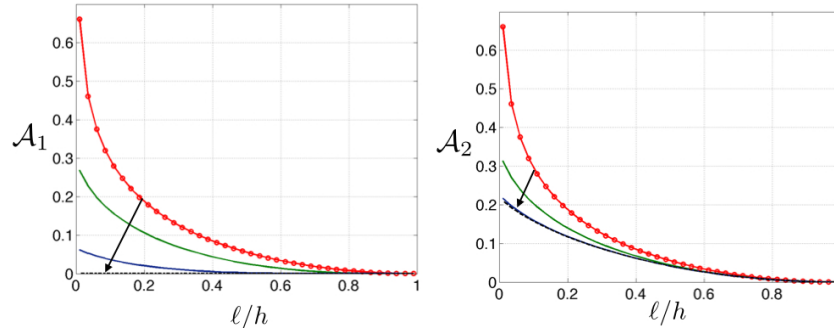

Fig. 9. Variations of $\mathcal{A}_1$ and $\mathcal{A}_2$ with ℓ/h. The arrow indicates increasing values of e/h ($e/h = 0, 0.1, 0.5$) and the asymptotic $e/h = 10$ is shown in dotted lines. For $e = 0$, open symbols show $\mathcal{A}_0$, Eq. (39).

As previously said, the case of vanishing thickness $e = 0$ is of practical importance in the actual design of metamaterials. In this case, the interface parameters have significant simplifications, with $\mathcal{A}_1 = \mathcal{A}_2 = \mathcal{A}_0$, and

$$
\mathcal{A}_0 = -\frac{1}{2\pi}\log\left(\sin\frac{\pi}{2}\ell\right).
\tag{38}
$$

REFERENCES

1. D. R. Smith and J. B. Pendry, "Homogenization of metamaterials by field averaging," JOSA B **23**, 391–403 (2006).
2. J. Mercier, M. Cordero, S. Félix, A. Ourir, and A. Maurel, "Classical homogenization to analyze the dispersion relations of spoof plasmons with geometrical and compositional effects," Proc. R. Soc. A **471**, 20150472 (2015).
3. A. Căbuz, A. Nicolet, F. Zolla, D. Felbacq, and G. Bouchitté, "Homogenization of nonlocal wire metamaterial via a renormalization approach," JOSA B **28**, 1275–1282 (2011).
4. C. Fietz, "Electro-magnetostatic homogenization of bianisotropic metamaterials," JOSA B **30**, 1937–1944 (2013).
5. R. V. Craster, J. Kaplunov, E. Nolde, and S. Guenneau, "High-frequency homogenization for checkerboard structures: defect modes, ultrarefraction, and all-angle negative refraction," JOSA A **28**, 1032–1040 (2011).
6. C. R. Simovski, "On electromagnetic characterization and homogenization of nanostructured metamaterials," Journal of Optics **13**, 013001 (2011).
7. Y. Capdeville and J.-J. Marigo, "Second order homogenization of the elastic wave equation for non-periodic layered media," Geophysical Journal International **170**, 823–838 (2007).
8. Y. Capdeville, L. Guillot, and J.-J. Marigo, "2-d non-periodic homogenization to upscale elastic media for p–sv waves," Geophysical Journal International **182**, 903–922 (2010).
9. J.-J. Marigo and C. Pideri, "The effective behavior of elastic bodies containing microcracks or microholes localized on a surface," International Journal of Damage Mechanics p. 1056789511406914 (2011).
10. M. David, J.-J. Marigo, and C. Pideri, "Homogenized interface model describing inhomogeneities located on a surface," Journal of Elasticity **109**, 153–187 (2012).
11. A. E. Minovich, A. E. Miroshnichenko, A. Y. Bykov, T. V. Murzina, D. N. Neshev, and Y. S. Kivshar, "Functional and nonlinear optical metasurfaces," Laser & Photonics Reviews **9**, 195–213 (2015).
12. G. Goussetis, A. P. Feresidis, and J. Y. C. Vardaxoglou, "Tailoring the amc and ebg characteristics of periodic metallic arrays printed on grounded dielectric substrate," Antennas and Propagation, IEEE Transactions on **54**, 82–89 (2006).
13. B. O. Zhu, J. Zhao, and Y. Feng, "Active impedance metasurface with full 360 [deg] reflection phase tuning," Scientific reports **3** (2013).
14. A. Pors, O. Albrektsen, I. P. Radko, and S. I. Bozhevolnyi, "Gap plasmon-based metasurfaces for total control of reflected light," Scientific reports **3** (2013).
15. F. Costa, S. Genovesi, A. Monorchio, and G. Manara, "A circuit-based model for the interpretation of perfect metamaterial absorbers," Antennas and Propagation, IEEE Transactions on **61**, 1201–1209 (2013).

16. O. Luukkonen, C. Simovski, G. Granet, G. Goussetis, D. Lioubtchenko, A. V. Räisänen, S. Tretyakov *et al.*, "Simple and accurate analytical model of planar grids and high-impedance surfaces comprising metal strips or patches," Antennas and Propagation, IEEE Transactions on **56**, 1624–1632 (2008).

17. M. Beruete, M. Navarro-Cía, F. Falcone, I. Campillo, and M. Sorolla, "Single negative birefringence in stacked spoof plasmon metasurfaces by prism experiment," Optics letters **35**, 643–645 (2010).

18. G. Bouchitte and R. Petit, "On the concepts of a perfectly conducting material and of a perfectly conducting and infinitely thin screen," Radio Science **24**, 13–26 (1989).

19. R. Petit, G. Bouchitte, G. Tayeb, and F. Zolla, "Diffraction by one-dimensional or two-dimensional periodic arrays of conducting plates," in "San Diego,'91, San Diego, CA," (International Society for Optics and Photonics, 1991), pp. 31–41.

20. A. Maurel, J.-F. Mercier, and S. Félix, "Wave propagation through penetrable scatterers in a waveguide and through a penetrable grating," The Journal of the Acoustical Society of America **135**, 165–174 (2014).

21. A. Maurel, J.-F. Mercier, and S. Félix, "Modal method for the 2d wave propagation in heterogeneous anisotropic media," JOSA A **32**, 979–990 (2015).

22. S. Tretyakov, *Analytical modeling in applied electromagnetics* (Artech House, 2003).

23. P. A. Martin and R. A. Dalrymple, "Scattering of long waves by cylindrical obstacles and gratings using matched asymptotic expansions," Journal of Fluid Mechanics **188**, 465–490 (1988).